Multi-hand Frequency Selective Surface wi(h Multi-Ring Patch Elements

Te-Kao Wu
Jet Propulsion Laboratory
California Institute of Technology
Pasadena, California 91109

Shung-Wu Lee
University of Illinois
Urbana, Illinois 61801

Abstract

Theoretical analysis and experimental verifications are presented for a multi-band frequency selective surface (FSS) with perfectly conducting multi-ring patch elements. Both the exact formulation and the thin-ring approximation are described for analyzing and designing this multi-ring patch element FSS. It is found that the thin-ring approximation fails to predict the electrically wide ring element FSS's performance. A single screen double-ring clement FSS is demonstrated for (1) a low-pass FSS that reflects the Ka-band signal while passing the S-, X-, and Ku-band signals, and (2) a tri-band system that reflects the X-band signal while transmitting through the S- and Ku-band signals. In addition, a double screen FSS with non-similar double-ring elements is presented for the Cassini's four-band system which reflects the X- and Ka- band signals while passing the S- and Ku-band signals. . . The good agreement obtained between the measured and the computed results verified the , single cascading mode approach of this paper.

1. Introduction

Frequency selective surfaces (FSS) have often been considered for the reflector antenna applications [1-7]. Typically, an FSS is employed for the subreflector and the different frequency feeds are optimized independently and placed at the real and virtual foci of the subreflector. Hence, only one single main reflector is required for the multi-frequency operation. For example, the FSS on JPL's Voyager spacecraft high gain antenna (HGA) was " designed to diplex S and X bands [1]. in that application the S-band feed is placed. at the prime focus of the main reflector, and the X-band feed is placed at the Cassegrain focal point, Note that only one main reflector is required for this two band operation. Thus, tremendous reduction in mass, volume and, most important, the cost of the antenna system are achieved with the FSS subreflector.

in the past, the cross-dipole patch clement FSS was used for the subreflector design in the reflector antennas of Voyager [1] for reflecting the X-band waves and passing the S-band waves, and the Tracking and Data Relay Satellite System (TDRSS) for diplexing the S- and Ku-band waves [2]. The characteristics of the cross-dipole clement FSS changes drastically as the incident angle is steered from normal to 40°. Thus a large band separation is required to minimize the RF losses for these dual band applications. This is evidenced by the reflection 'and transmission band ratio (f_r/f_t) being 7:1 for single screen FSS [2] or 4:1 for double screen FSS [1] with cross-dipole. patch elements. Better elements, such as the. concentric-circular or square loop elements [3-10] are definitely needed to achieve (1) the. multiplexing of four frequency bands, (2) smaller frequency-band separations (f_t/f_r less than 1 .7), and (3) less sensitivity to the incident angle variation and polarizations.

Recently, NASA's Cassini project required the use. of multiple microwave frequencies at S, X, Ku and Ka bands for science investigations and data communication links. A single HGA with an FSS subreflector, as illustrated in Figure 1, was proposed. This arrangement

allows a Cassegrain configuration at X (7.2 and 8.4 GHz) and Ka (32 and 34.5 GHz) bands and a prime. focus configuration at S (2.3 GHz) and Ku (13.8 GHz) bands [5-8]. Circular polarizations are. required for all frequency bands except the Ku-band. To meet the Cassini antenna subsystem's RF requirements, two design approaches as shown in Figure 2, are proposed. In addition, the FSS screen was bonded on to a Kevlar honeycomb panel to meet the mechanical and thermal environmental requirements.

The first approach, implementing the two-screen design, uses two FSS grids. The front FSS grid is called Ka-add-on FSS. It reflects Ka-band waves but passes S-, X- and Ku-band waves. The back FSS grid is called the 3-frequency FSS. It reflects X-band waves but passes S- and Ku-band waves. The resultant FSS rc.fleets both X- and Ka-band waves but passes both S and Ku band waves. The second approach, implementing the single screen design, uscs only a single FSS grid to reflect the X- and Ka-band waves and to pass the S- and Ku-band waves. in this paper the analysis, design and performance of a four-frequency FSS (S/X/Ku/Ka bands) with multi-ring elements are. demonstrated. The selection of the concentric multi-ring elements is because the ring's geometry conforms to the circular polarization requirement of the Cassini project and it is easy to manufacture.

II. Analysis of a Single Screen Multi-ring FSS

A modal analysis of a single screen FSS with circular ring patch element was presented by Parker, et al [9-13]. However, their analysis is limited to thin rings with dielectric substrates on onc side of the metallic. screen only. For the present multi-band application, *wider* rings arc required. Hence a more exact theory is developed for rings with an arbitrary width and multiple layers of dielectrics on both sides of the. grid, as illustrated in Figure 3. The theory is similar to the. standard modal analysis published by Chen [9], Lee [10], and by Roberts and McPhedran [14]. The expansion function used to represent the

current on the ring is related to the modal field in a coaxial waveguide via the Babinet principle.. The validity of this analysis and the convergence of these expansion functions will also be discussed.

in the theoretical model, as shown in Figure 3, the FSS is assumed to be a two-dimensional periodical array of conducting multi-ring patch elements. The fields in the free space region and the dielectric slabs are represented by the Floquet rnodc expansions. The unknown current J_s on the ring clement is represented by

$$\vec{J} = \frac{2}{\eta_o} \hat{z} \times \vec{E}_{com} \tag{1}$$

where η_o is the free-space wave impedence and E_{com} is the electric field in the annular aperture. of a complementary screen with infinite size and perfect conductivity.

$$\vec{E}_{com} = \sum_m \sum_n \{(C^v_{mn} + D^v_{mn})\ \vec{U}^v_{mn} + (C^h_{mn} + D^h_{mn})\ \vec{U}^h_{mn} + \frac{\Gamma_{mn}}{k_o} (\bar{C}^v_{mn} - \bar{D}^v_{mn})\ \vec{V}^v_{mn} + \frac{\Gamma_{mn}}{k_o} (\bar{C}^h_{mn} - \bar{D}^h_{mn})\ \vec{V}^h_{mn}\} \tag{2}$$

where C and D are the unknown coefficients to be determined, and U and V are the field expan sion functions (or bases functions). The superscripts v and h indicate vertically and horizontally polarized components, as defined in [15]. The summation in Equation (2), -- includes the superposition of currents on all the rings of the multiple-ring element, as shown in Figure 3. Next, the expansion function may be expressed in terms of the coaxial waveguide modes [15] as follows:

$$\begin{bmatrix} \vec{U}^v_{mn} \\ \vec{U}^h_{mn} \end{bmatrix} = \hat{\rho}\ \frac{m}{\rho}\ Z_m\ (\chi'_{mn}\ \frac{\rho}{c}) \begin{bmatrix} \sin m\phi \\ -\cos m\phi \end{bmatrix} + \hat{\phi}\ \frac{\chi'_{mn}}{c} Z'_m\ (\chi'_{mn}\ \frac{\rho}{c}) \begin{bmatrix} \cos m\phi \\ \sin m\phi \end{bmatrix} \tag{3}$$

$$\begin{bmatrix} \vec{V}^v_{mn} \\ \vec{V}^h_{mn} \end{bmatrix} = -\hat{\rho}\ \frac{\chi_{mn}}{c}\ \bar{Z}'_m\ (\chi_{mn}\ \frac{\rho}{c}) \begin{bmatrix} \sin m\phi \\ \cos m\phi \end{bmatrix} + \hat{\phi}\ \frac{m}{\rho}\ \bar{Z}_m\ (\chi_{mn}\ \frac{\rho}{c}) \begin{bmatrix} -\cos m\phi \\ \sin m\phi \end{bmatrix} \tag{4}$$

where

$$\Gamma_{mn} = \left[k^2 - \left(\frac{\chi'_{mn}}{c}\right)^2\right]^{1/2}$$

χ'_{mn} = nth root of $Z'_m(\tau\chi'_{mn})$, the derivative of the Bessel-Neumann combination,

$$Z'_m\left(\chi_{mn}\frac{\rho}{c}\right) = Q_1\left[J_m\left(\chi'_{mn}\frac{\rho}{c}\right)N'_m\left(\chi'_{mn}\right) - N_m\left(\chi_{mn}\frac{\rho}{c}\right)J'_m\left(\chi'_{mn}\right)\right]$$

$$Q_1 = \pi\sqrt{30}\,\epsilon_m\left\{\left|\frac{J'_m(\chi'_{mn})}{J'_m(\tau\chi'_{mn})}\right|\left|1 - \left|\frac{m}{\tau\chi'_{mn}}\right|^2\right| - |1 - \left|\frac{m}{\chi'_m}\right|^2|\right\}^{-1/2}$$

$$\epsilon_m = \begin{cases}1, & \text{if } m = 0\\ 2, & \text{if } m \neq 0\end{cases}$$

$$\bar{Z}_m\left(\chi_{mn}\frac{\rho}{c}\right) = Q_2\left[J_m\left(\chi_{mn}\frac{\rho}{c}\right)N_m(\chi_{mn}) - N_m\left(\chi_{mn}\frac{\rho}{c}\right)J_m(\chi_{mn})\right]$$

$$Q_2 = \pi\sqrt{30\,\epsilon_m}\left\{\left[\frac{J_m(\chi_{mn})}{J_m(\tau\chi_{mn})}\right]^2 - 1\right\}^{1/2}$$

$\tau = \frac{d}{c}$, where d ancl c are defined in Figure 2.

in the. case when the width of the ring is electrically small, the following simplified] expression can be used for the field expansion function of (2):

$$\vec{U}_m^{v,h} = \hat{\rho}\,\frac{1}{\rho}\left[\frac{\epsilon_m\,60}{\ln(d/c)}\right]^{1/2}\begin{bmatrix}\sin m\phi\\ \cos m\phi\end{bmatrix} \qquad (5)$$

$$\vec{V}_m^{v,h} = 0.$$

A matrix equation may bc formulated by matching the following three boundary conditions at the region that contains the ring elements: (1) the tangential E fields are continuous at z = O; (2) the current on the metallic rings $J_s = \hat{z} \times [H_t(0^+) - H_t(0^-)]$; (3) cm the metallic rings, the tangential E field = O. "l'his matrix equation allows the determination of the unknown coefficients C and D for the current J_s on the metallic rings. Once the current is found, the incident and reflection coefficients at each dielectric interface. can be calculated. Finally, the reflection and transmission coefficients (R_{pq} and T_{pq}) of the overall FSS can also be calculated, which will lead to the determination of the reflected and transmitted fields.

Two computer codes were developed based on the above analysis. MRINGC code is limited for thin ring element, since it is based on the thin wire approximation (Eq. 5), i.e. the ring current has no radial variation nor components. However, MRING2C code is not limited, since it is based on the exact waveguide modal fields shown earlier. To check the convergence rate and the accuracy of the codes, the resonant frequency of the single ring clement FSS on a 0.075 mm thick polyester was computed using the MRINGC code and compared to the measured results of [11]. The geometric dimensions of this FSS grid arc (see Figure 3) a=b=4.9 mm, c= 1.95 mm, d=2.25 mm. Table 1 summarizes the number of Floquet modes needed for different dielectric constant of the substrate. Here the current expansion mode number is seven, Note that the results converge, as 625 Floquet modes arc used. Furthermore, in Reference [11], it is stated that the same FSS etched on a polyester substrate (with 2.33 dielectric constant) is resonant at 22 GHz. However, from Table 1, in order to get the same resonant frequency at 22 GHz as in [11], the dielectric constant must be 3.5 instead of 2.33. For the MRING2C code, seven terms in the current expansion of Eq. (1) are sufficient to obtain the convergent results.

111. Single Screen Low-Pass (Ka-add-on) FSS

A single screen, single ring element FSS was fabricated on a 3 mil thick Kapton, as shown in Figure 4. The good agreement between the computed and measured transmission performance of this FSS is illustrated in Figure 5. The computed data was obtained by running the MRINGC code, since the width of the ring is only 2 roil. This verified the accuracy of the MRIGC code.

Next a single screen FSS with one to four-ring as the element were studied. The double ring (DR) element FSS was found to give the best result. Figure 6 shows the comparison of single ring and double ring element FSS. Note that the double ring clement FSS has a much sharper transition from pass band to stop band, and the radius r_1 (or r_2) is the inside radius of the larger ring (or the smaller ring). The resonant frequency of the DR1 FSS shifts down when the inner ring is added to the same size single ring clement FSS. By reducing the DR1 clement's size, the DR2 FSS has the same resonant frequency as the single. ring FSS. However the losses at Ku and X bands are much smaller than the single ring FSS. Therefore, the double ring FSS should provide better performance. in a low-pass FSS design.

Figure 7 gives the computed transmission performance of this DR2 FSS on the same. Kevlar honeycomb panel as in Figure 2, for incident angles steered from normal to 45°. Note. that the resonant frequency shifted about 1.5 GHz. Improved performance can be obtained from a double ring clement FSS with a triangular lattice, as shown in Figure 8. This new FSS's resonant. frequency shifted only about 1 GHz as the incident angle varied from normal to 45°. Note the double-ring patch element array is etched on a 0.002" thick Kapton sheet with 0.029 ounce/ft^2 copper and then bonded to the Kevlar honeycomb pane]. The computed results arc obtained using the MRIG2C code, because the ring width is fairly wide at Ka-band frequencies. Only representative measure.d data at 30° TE incidence is

given here to demonstrate the good agreement between the computed and measured data.

IV. Single Screen Tri-Band (3-Frequency) FSS

Similarly, the three-frecplency FSS design and performance are given in Figure 9. Again the double-ring patch element array is etched on a 0.002" thick Kapton sheet with 0.029 ounce/ft^2 copper and then bonded to the Kevlar honeycomb panel of Figure 2. Since the width of the rings are. small compared to the radii, the computed results may be obtained by either the thin-ring or the wide-ring FSS code. Only representative measured data at 0° (normal) incidence is given hex-e to demonstrate the agreement between the computed and measured data. As can be observed from this figure, the resonant frequency is very close to the designated 8.4 GHz for both TE and TM polarizations even when the incident angle is changed from norms] to 45°. 'l'his proves that the ring element FSS gives much bet ter performance than th c cross- dipole or the J erusalem-cross elements. The FSS's insertion losses at these three frequency bands arc summarized in TABLE 2. Note that the losses at 2.3 and 13.8 GHz are transmission losses, while they arc reflection losses at the other frequencies.

V. Single Screen 4-Frequency FSS

in general, the double-ring element FSS provides two resonances, i.e., one at a lower frequency (caused by the larger ring) and the other at a higher frequency (caused by the smaller ring). Therefore, one might be able to design a single screen DR FSS for the Cassini's 4-frequency FSS. Namely, only one DR FSS grid might be needed for reflecting the X- and Ka-band while passing the S- and Ku-band waves. To avoid the grating lobe occu rrence at Ka-band, the single. screen FSS is designed with a high dielectric constant (ϵ_r =11) Duroid 6010.5 substrate. The MRINGC (thin ring) code was next used to obtain the

DR FSS grid design.

Figure 10 shows the geometry and configuration of this DR FSS. To provide a pass-band at Ku-band, the width of the inner ring must be large. The computed transmission performance. of this DR FSS is illustrated in Figure 11 at S-, X- and Ku-band for incident angle steered from normal to 45°. Representative comparison data between the measured and computed results are shown in Figures 12 for 30° incidence only. Note that the computed results were obtained by running the MRINGC code, since the outer ring is 0.004" wide. At Ka-band, however, no agreement was obtained between the measured data and the computed results of the MRINGC code. This implies that the thin ring code cannot accurately predict the performance of an electrically wide ring FSS.

Thus the. MRING2C code is used to compute the transmission performance of this single screen DR FSS. Computed results arc illustrated in Figure 13 along with the representative measured results at 30° TE incidence. Here the agreement between the measured and computed results verified the accuracy of MRING2C code. Figure 13 also shows that at Ka-band no common reflection band can be found for both the TM and TE polarizations. This indicated that the single screen DR FSS is good only for a 3-frequency FSS application. For 4-frequency FSS applications, the two-screen design should be implemented with this double ring element FSS.

VI. Cascading Two Non-Similar Screens

in Section 11, equations were derived to analyze single. screen or double. screen FSS with multi-ring patch elements. This analysis can be further extended to analyze an integrated double screen FSS by employing the symmetry property and the technique of image theory [6]. In another words, the second FSS screen is the. exact duplicate of the first 1 'SS screen. However, Cassini's four-band FSS (S/X/Ku/Ka bands) needs double screen FSS

with non-similar design [8]. Namc]y, the FSS element designs, i.e. the clement geometrical dimensions (especially the periodicity and the lattice types), arc different for the two screens.

The cascading of two non-similar FSS screens is very difficult to analyze exactly. However, using the following systematic procedures, a single-rnode cascading approach may readily bc employed to get a first order assessment of this double-screen FSS's performance. Consider the double-scrccn FSS as shown in Figure 2b. First, one divides the FSS at the middle thickness of the Kevlar honeycomb. Upwards from this middle plane is considered the first FSS screen section, and below this plane is the second FSS screen section. Each FSS section can bc accurately modelled by the single screen FSS analysis described earlier. Since the dividing plane is electrically far from the FSS grid and the FSS clement spacing is less than a half wavelength, onc can assume that all the modes are decaying except the 0th order mode [19]. Thus onc may next cascade the two sections by converting the scattering matrix [s] from each section to a transmission matrix [t] and multiplying the resulting [t] matrices. The converting from [s] matrix to [t] matrix is the same as that described in [18]. The final [t] matrix product is then converted back to a scattering matrix, which yields th c transmission an c1 ref lection coefficients for the double screen FSS. Figure 14 shows th e comparison of the computed and measured transmission performance for this double screen FSS. The good agreemen t verified this ef ficient cascading approach. Th c double-screen FSS performane at all the Canssini frequencies is sumarized in Table 3.

Note that this single mode approximation is similar to the transmission-line cascading approach of [16,17]. The nice feature of this simplified approach is that the cascading analysis avoids the specific geometrical dimensions of the individual FSS screen. In other words, the single-mode cascading analysis depends only on the spacer between the two FSS screens and the 0th order scattering matrix of each individual screen. It should be pointed

out that this single-mode cascading analysis, however, is better than the transmission-line approach due to the fact that both co- and cross-polarization (i.e. TE and TM) components are being considered. Furthermore, the 0th order scattering matrix of each individual FSS screen is computed accurately with the analysis of Section 11.

VII. Conclusion

Analysis, design and test results arc presented for the multi-band FSS with multi-ring patch elements. Good agreement between the measured ancl computed results verifies the various design approaches described in this paper. It is found that the thin-ring approximation fails to predict the performance. of an electrically wide ring element FSS. To multiplex the Cassini's four frequency bands (S/X/Ku/Ka) only the double screen FSS approach can give satisfactory results. One may further simplify this double screen FSS design by the efficient single cascading mode approach described in Section VI.

Acknowledgement

The work described in this article was carried out by the J et propulsion Laboratory, California institute of Technology, under contract with the National Aeronautics and Space Administration. The authors wish to thank Dr. Ken Woo for the managerial support, Mr, G. Hicky for fabricating the. honeycomb sandwiches, and Mr. Cosine Chavez for taking th e FSS measurement.

REFERENCES

1. G.H. Schennum, "Frequency-sclcctivc surfaces for multiple frequency antennas," Microwave Journal, vol. 16, pp.55-57, 1975.

2. V.D. Agrawal ant] W.A. Imbriale, "Design of a dichroic Cassegrain subreflector," 11~~.1~~

Trans., vol. TAP-27, no.4, pp. 466-473, July 1979.

3. K. Ueno, et al, "Characteristics of FSS for a multi-band communication satellite", paper presented at the 1991 Int. IEEE AP-S Symposium, Ontario, Canada, June 1991.

4. S. W. Lee, et al, "Designs for the ATDRSS Tri-band reflector antenna," paper presented at the 1991 Int. IEEE AP-S Symposium, Ontario, Canada, pp. 666-669, June 1991.

5. T.K. Wu, "Double-square-loop FSS for multiplexing four (S/X/Ku/Ka) bands", paper presented at the 1991 Int. IEEE AP-S Symposium Digest, Ontario, Canada, June 1991.

6. J. Huang and S.W. Lee, "Tri-band FSS with circular ring elements," paper presented at the 1991 Int. IEEE AP-S Symposium Digest, Ontario, Canada, June 1991.

"J. T.K. Wu, et al, "Multi-ring element FSS for multi-band applications," paper presented at the 1992 Int. IEEE AP-S Symposium, Chicago, IL, July 1992.

8. T.K. Wu, M. Zimmerman and S.W. Lee, "Evaluation of frequency selective reflector antenna systems," Microwave and Optical Technology Letters, vol.6, n0.3, pp. 175-179, March 1993.

9. E. A. Parker and S.M.A. Hamely, "Rings as Elements for FSS," Electronics Letter, pp.612-614, Aug. 1981.

10. E. Parker, S. Hamdy and R. Langley, "Arrays of Concentric Rings as Frequency Selective Surf aces," Electronics Letters, vol. 17, no. 23, 1981, p.880.

11. S. Hamdy, "Modal analysis of periodic arrays of simple and concentric rings as elements for FSS," Proc. Nat. Rad. Sci. Symp. EM Waves, Cairo, p.1 15, 1983.

12. E. A. Parker and J. C. Vardaxoglou, "Plane-Wave Illumination of Concentric-Ring Frequency-Selective Surf aces," IEE Proceedings, Vol. 132, pt. 11, P. 176, June 1985.

13. E. A. Parker and J. C. Vardaxoglou, "Influence of Single and Multiple-Layer Dielectric Substrates on the Band Spacings Available from a Concentric Ring Frequency-Selective Surface)" International Journal of Electronics, Vol. 61, PP. 291-297, 1986.

14. A. Roberts and R. McPhedran, "Bandpass Grids and Annular Apertures," IEEE Trans. Antenna and Propag., Vol. AP-36, 1'.607, May 1988.

15. N. Marcuvitz, Waveguide Handbook, Boston Technical Publishers, Inc., PP. 72-80, 1964.

16. T.K. Wu, "Frequency selective surfaces with rectangular/square elements," Int. IEEE AP-S Symp., Vancouver, Canada, June 1985.

17. C.C. Chen, "Diffraction of electromagnetic waves by a conducting screen perforated with circular holes," IEEE Trans. MTT- 19, pp. 475-481, May 1971.

18. S. Ramo, ct. a]., Fields ant] Waves in Communication Electronics, John Wiley & Sons, Inc., N. Y., 1965, p.605.

19. J. Vacchione and T.K. Wu, "Analysis of a dual, non-similar, screen FSS using simple cascading procedures," paper presented at the 1992 Int. IEEE AP-S Symposium, Chicago, Illinois, July 1992.

TABLE 1. Convergence St u dy for th e Resonant Frequ ency of a Single Screen FSS with Single Ring Patch Element

Dielectric Const ant	Floqu et Mode Number			
	81	289	625	1089
2.33	24.3(GHz)	23.8	23.1	23.1
3.5	23.0	22.0	22.0	22.0
4.0			21.6	21.6

TABLE 2. Insertion Loss (dB) Summary of the 3-Frequency FSS

Frequency (GHz)	$(\Theta_i, \phi_i) = (0°,0°)$	(30°, 0°)		(45°, 0°)	
		TE	TM	TE	TM
2.0	0.5	0.57	0.4	0.72	0.27
7.0	0.25	0.5	0,61	0.46	1.0
8.5	0.14	0.12	0.16	0.11	0.17
14.0	0.26	0.29	0.28	0.36	0.24

TABLE 3. Insertion Loss (dB) Summary of the Integrated Double Screen FSS Model.

Frequency (GHz)	$(\Theta_i, \phi_i) = (0°, 0°)$	(30°, o")		(45°, 0°)	
		TE	TM	TE	TM
2.3	0.71	0.71	0.5	0.8	0.3
7.2	0.43	0.33	0.42	0.37	0.88
8.4	0.13	0.11	*0.15*	0.11	0.18
13.8	0.54	0.82	*0.57*	0.94	0.39
32	*0.69*	0.62	0.71	0.52	0.76
34.5	1.09	1.24	1.82	1.29	2.1

FIGURE 1. PROPOSED CASSINI HIGH GAIN ANTENNA WITH A FOUR FREQUENCY FSS

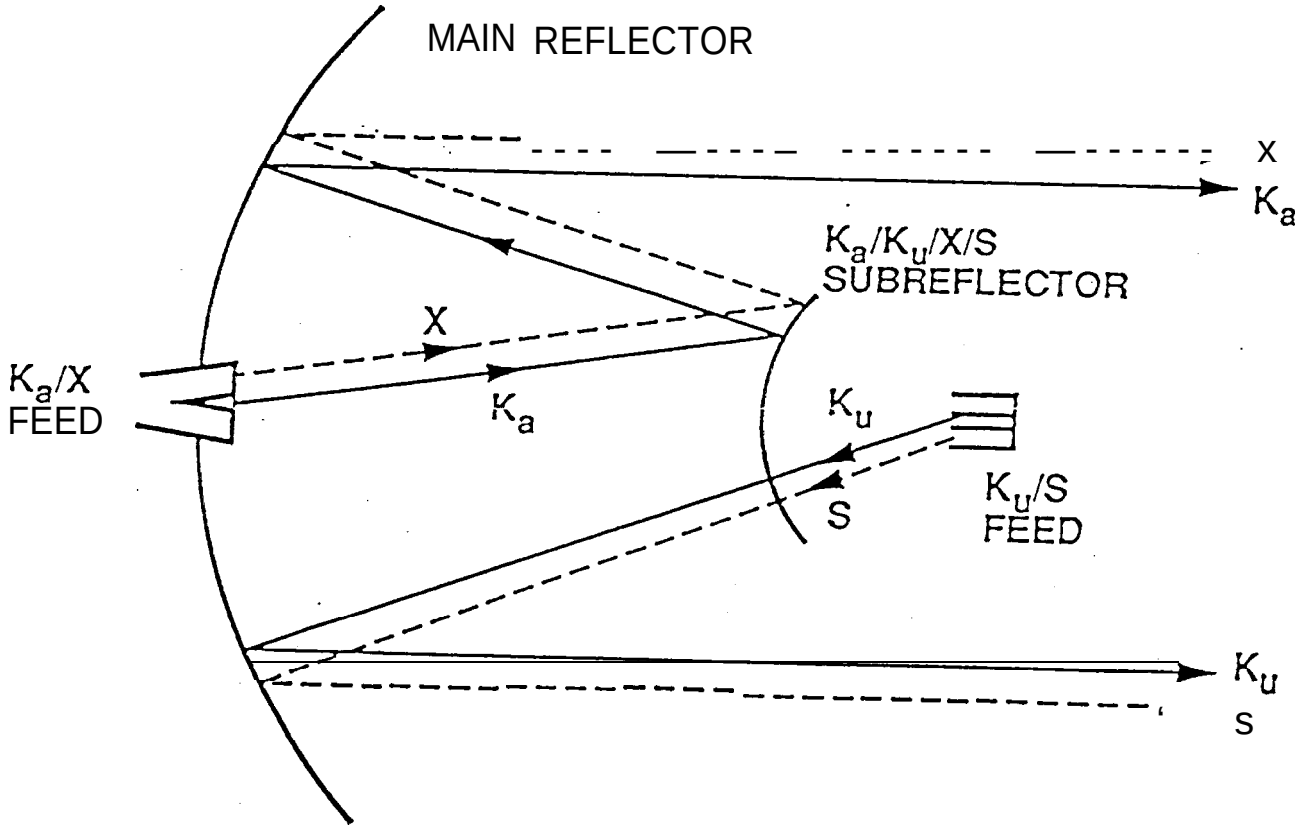

(a)

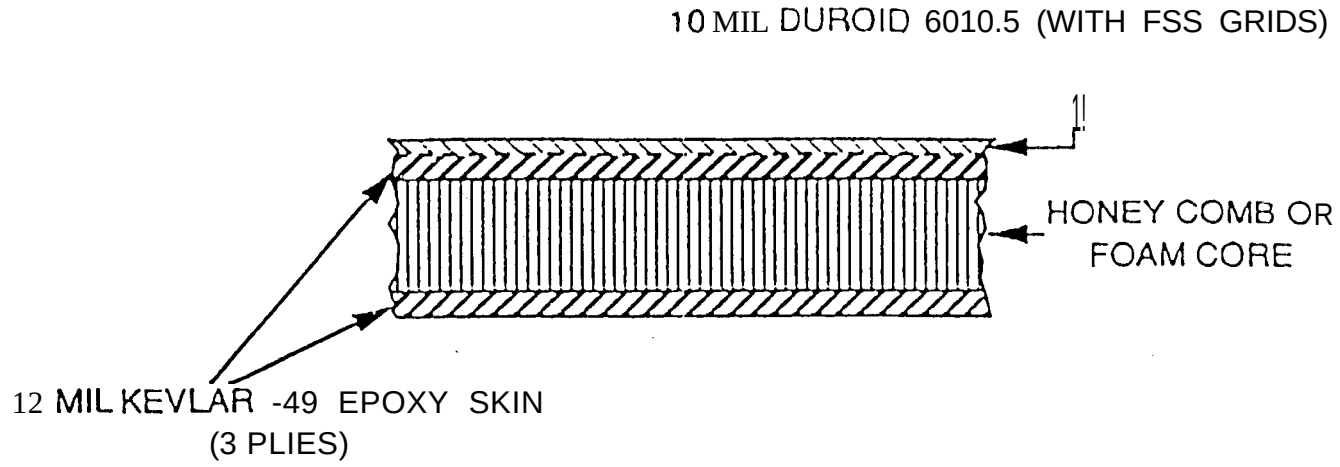

SINGLE SCREEN DESIGN

(b)

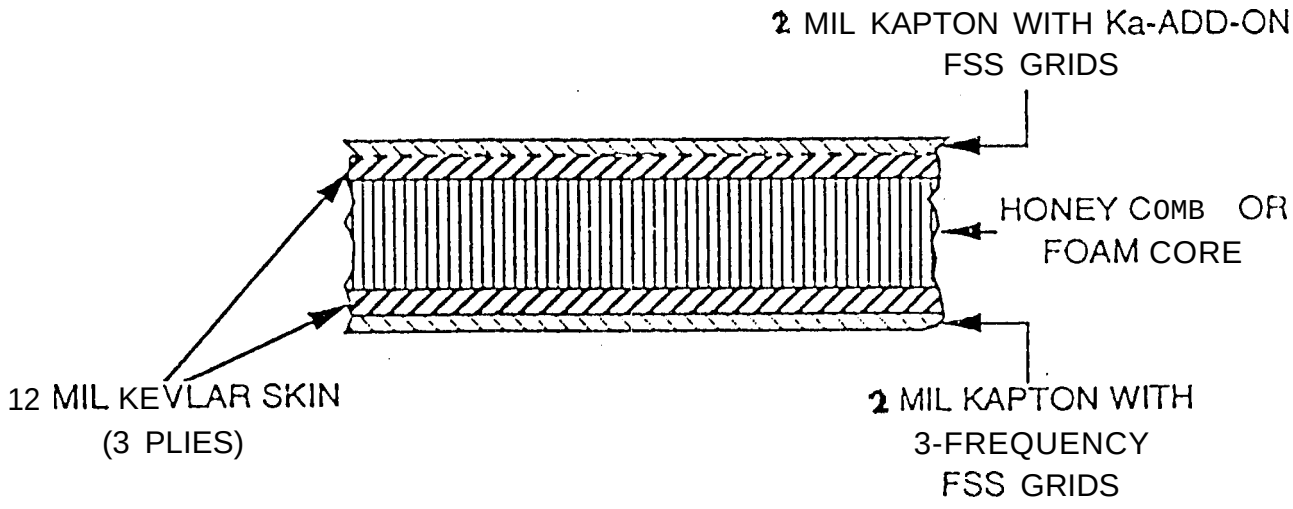

DOUBLE SCREEN DESIGN

Figure 2 Cassini's FSS Design Approaches

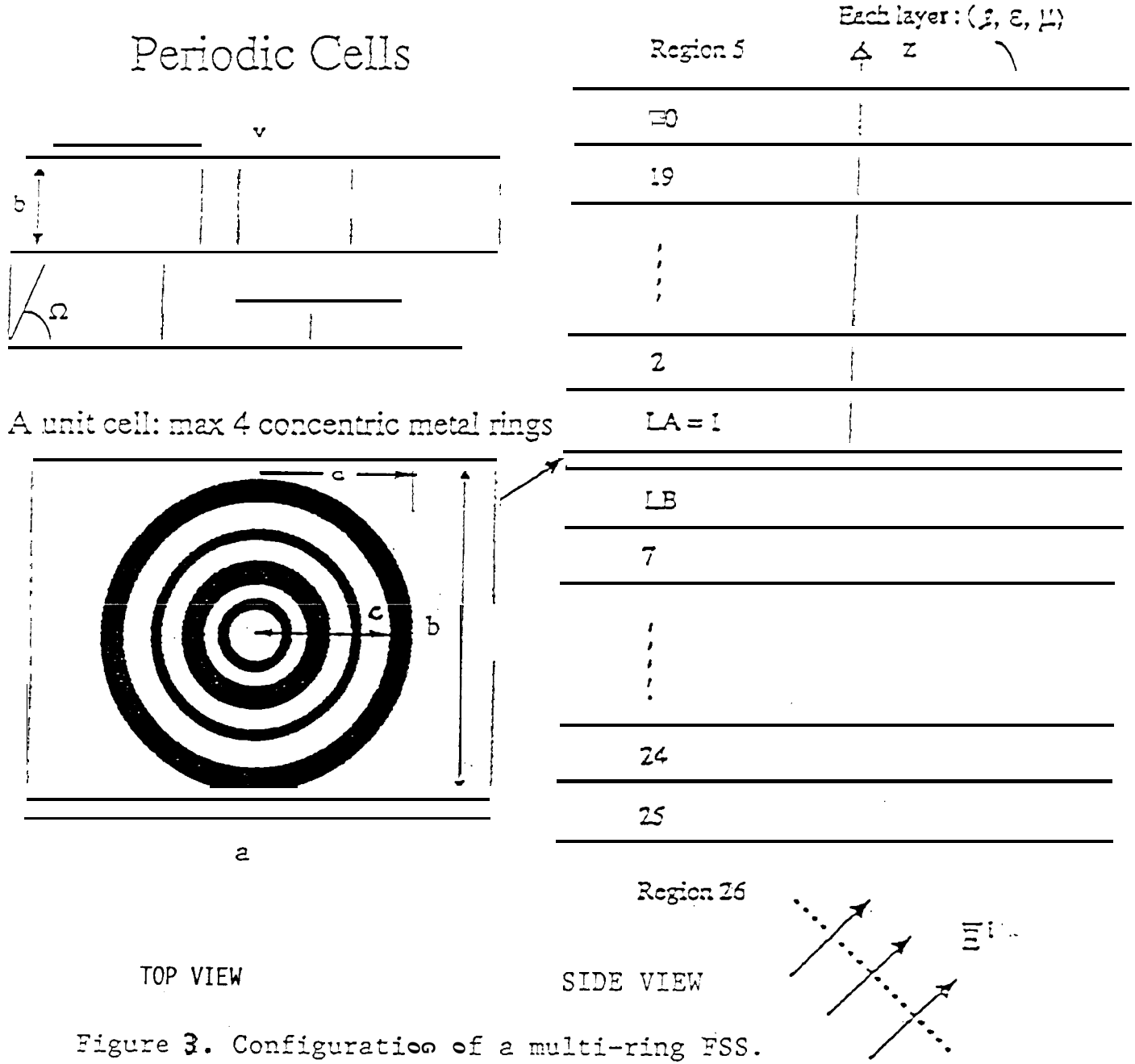

Figure 3. Configuration of a multi-ring FSS.

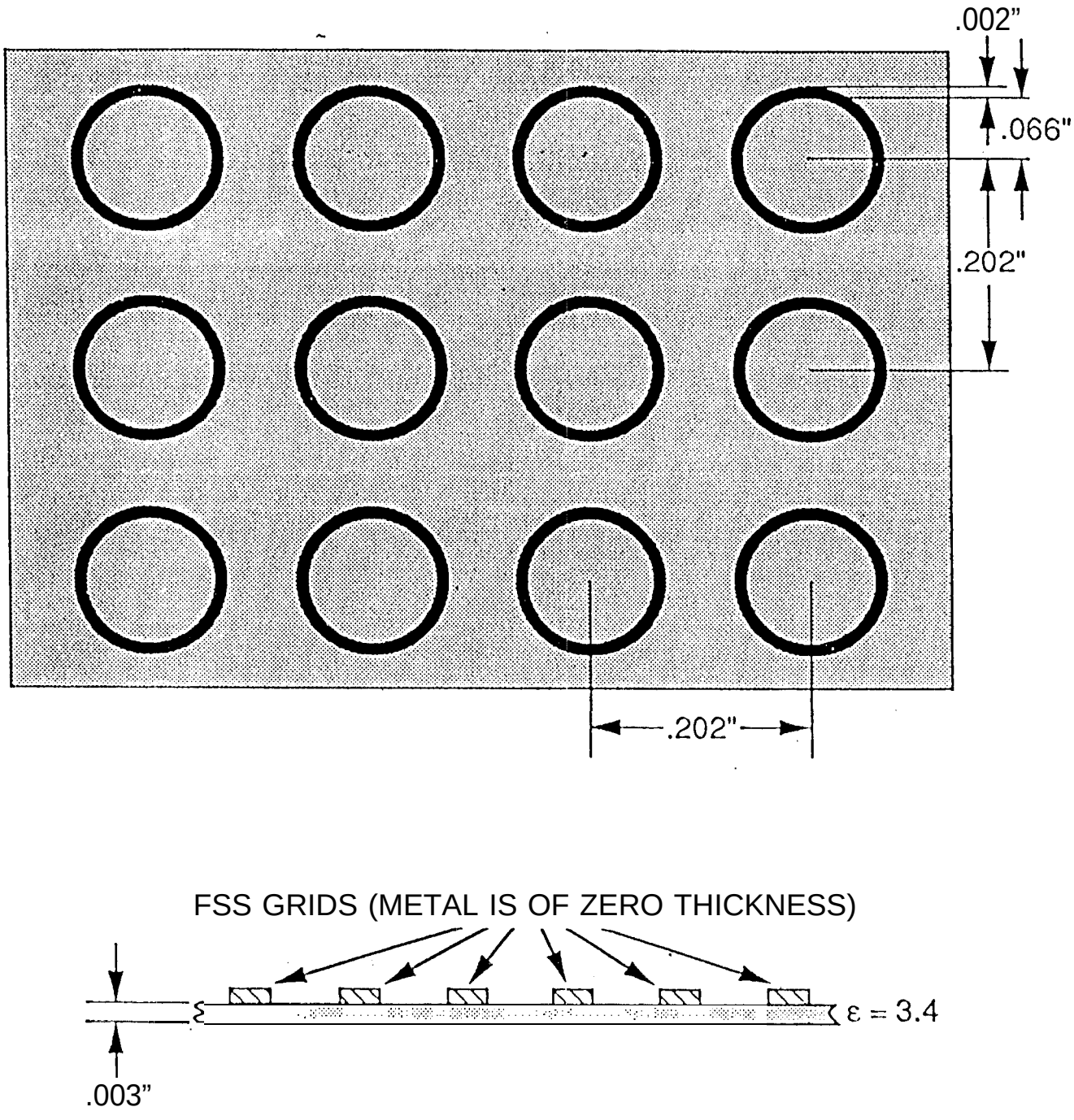

Figure 4. Configuration of the single ring element FSS.

FIGURE 5. COMPARISON OF COMPUTED AND MEASURED TRANSMISSION PERFORMANCE OF THE SINGLE RING FSS OF FIGURE 4 AT NORMAL INCIDENCE

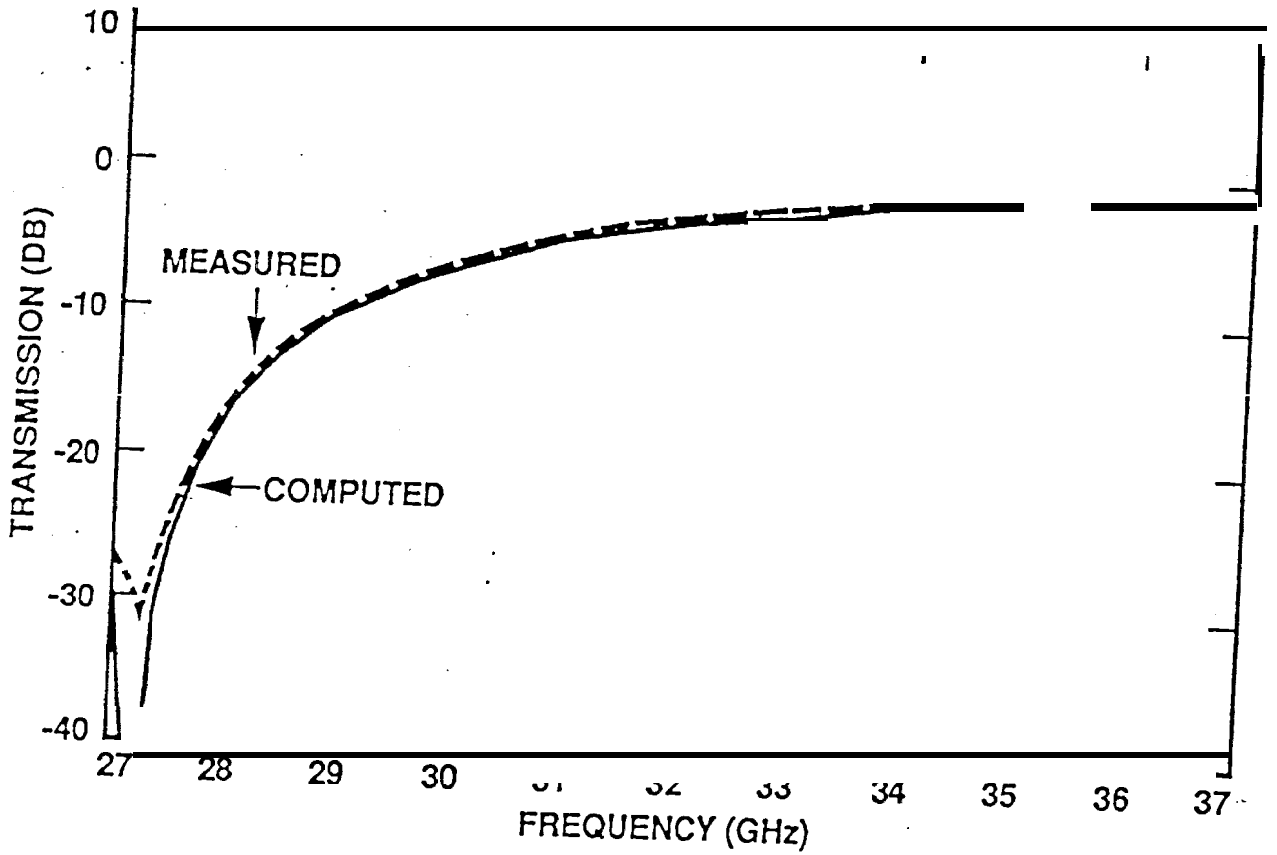

Figure 6. COMPARISON OF FSS TRANSMISSION PERFORMANCE BETWEEN SINGLE AND DOUBLE RING ELEMENTS, NORMAL INCIDENCE

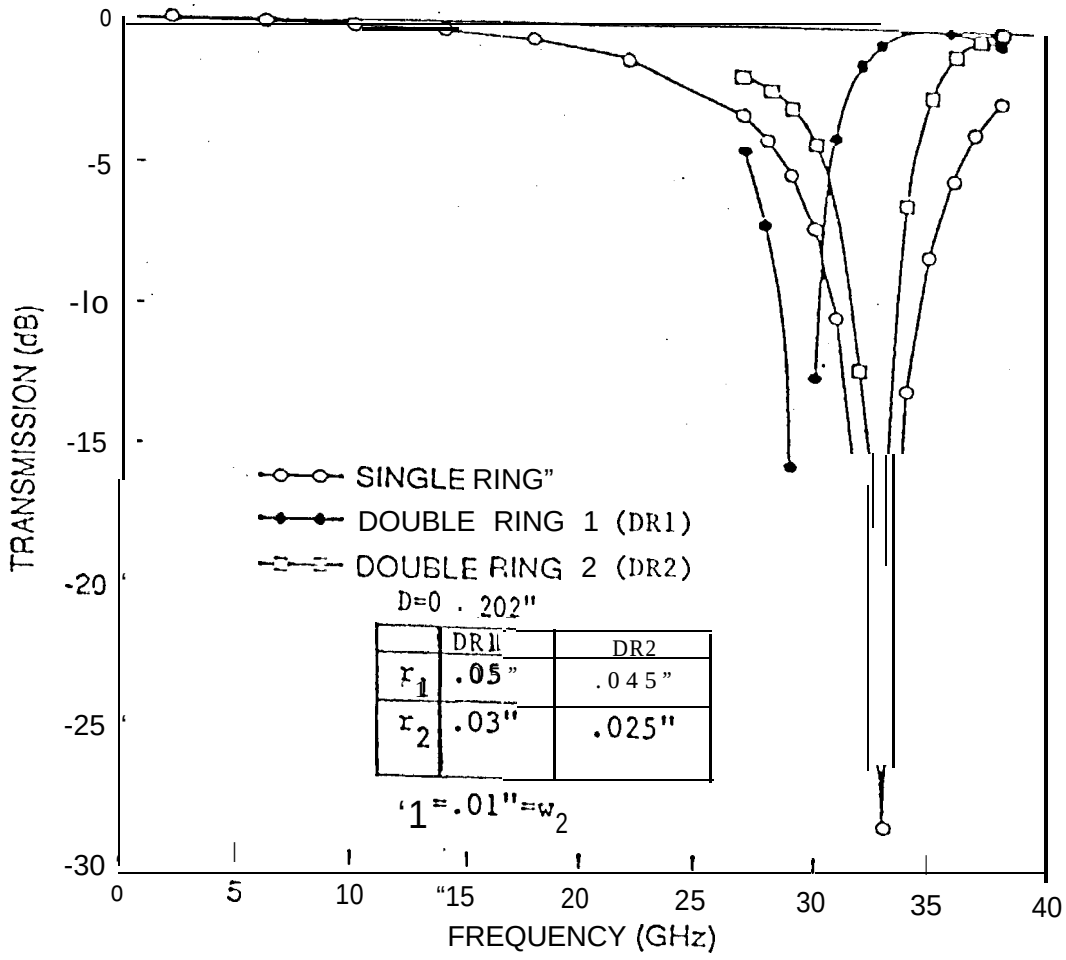

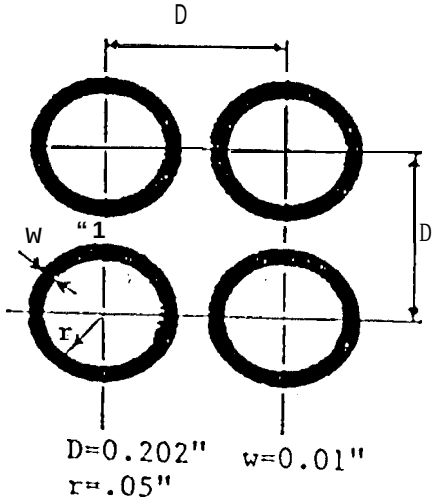

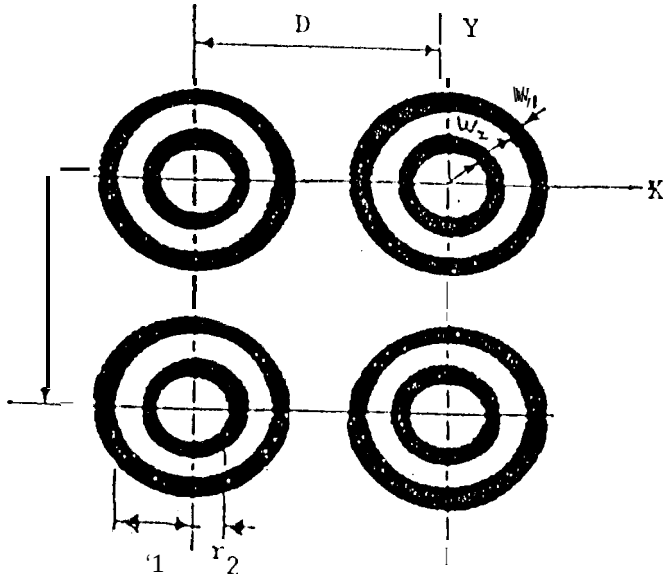

Figure 7. Computed transmission performance of a double ring element FSS.

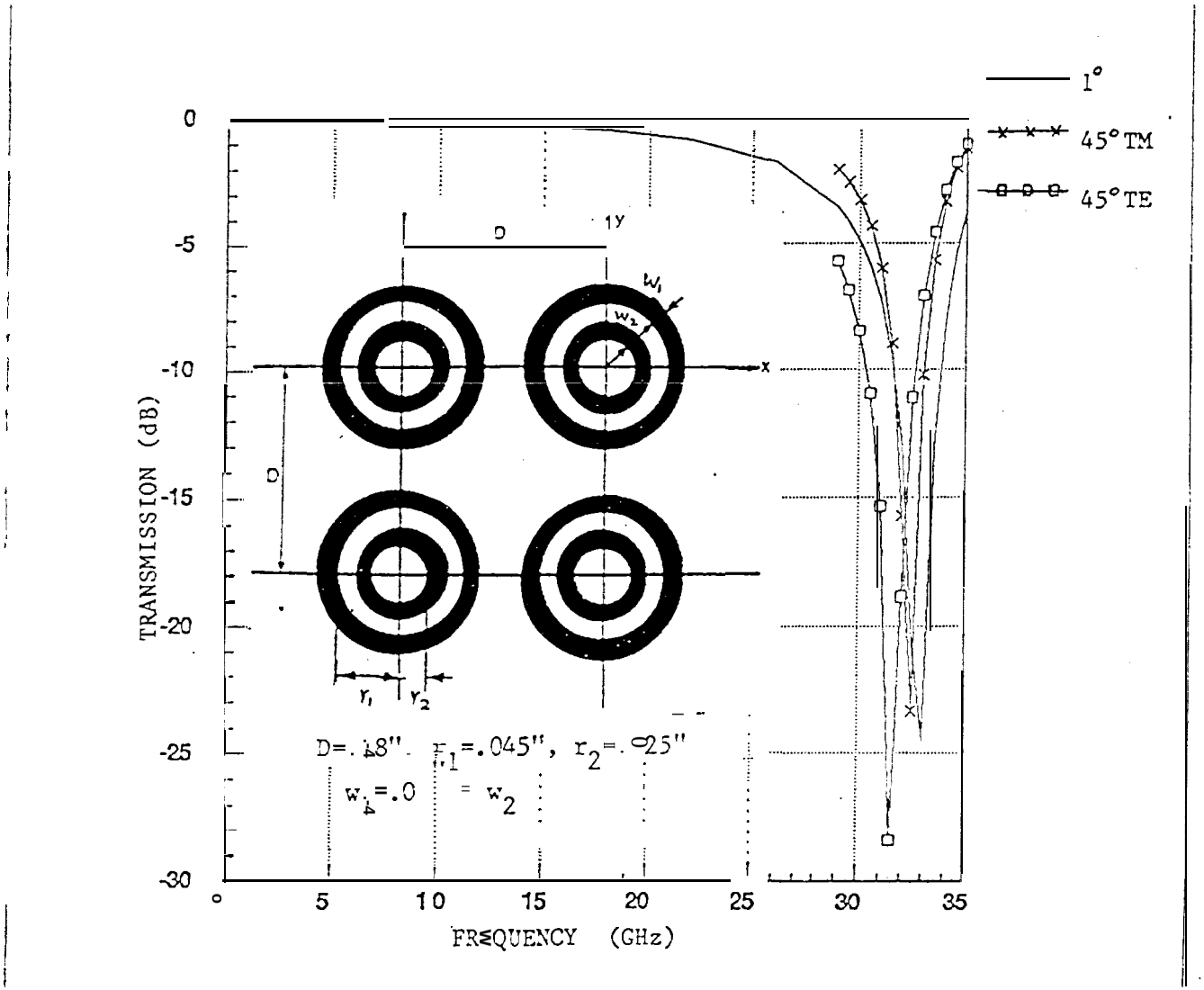

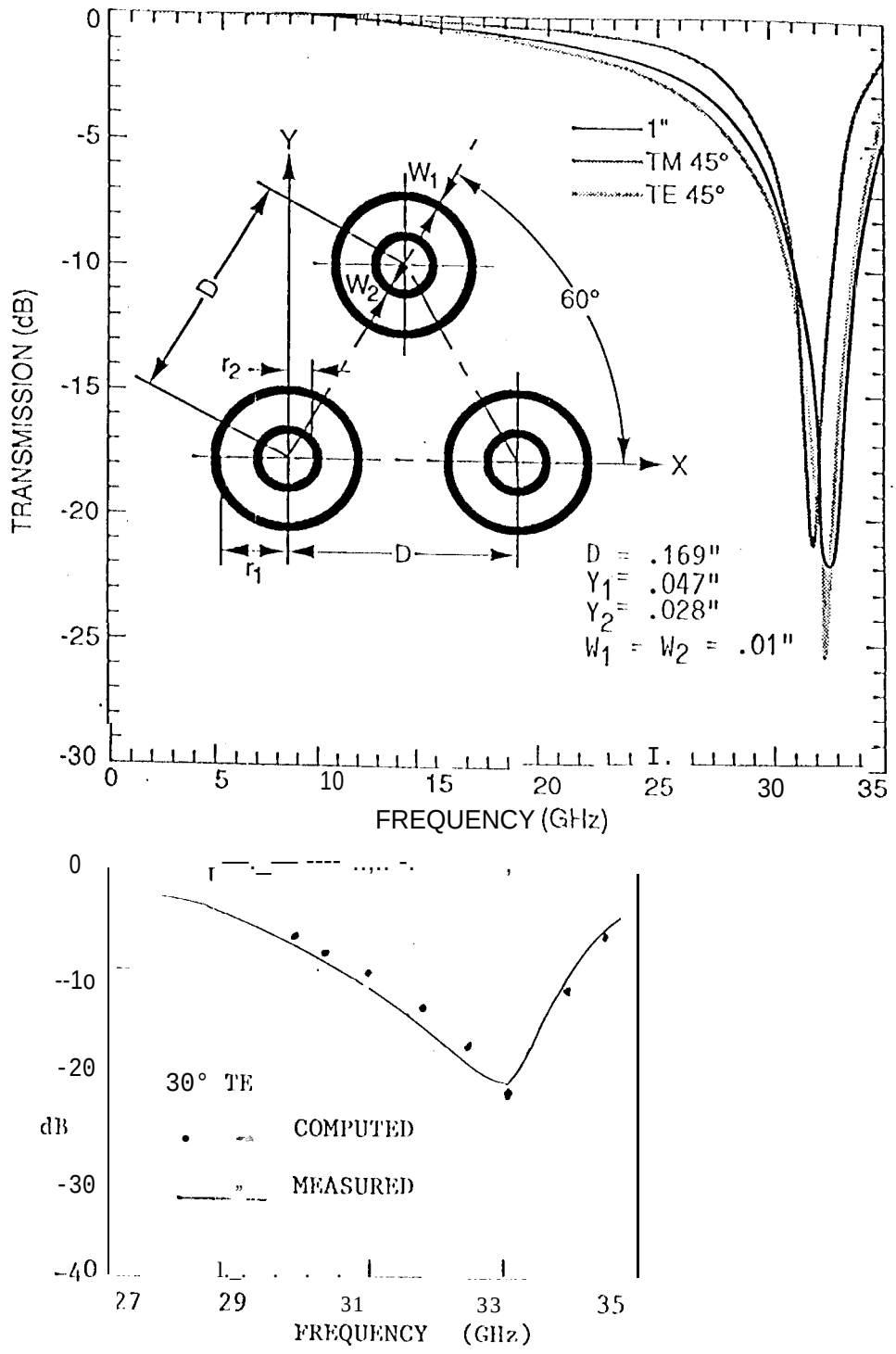

Figure 8. Design and transmission performance of the Ka-acid-otl FSS with double-ring element.

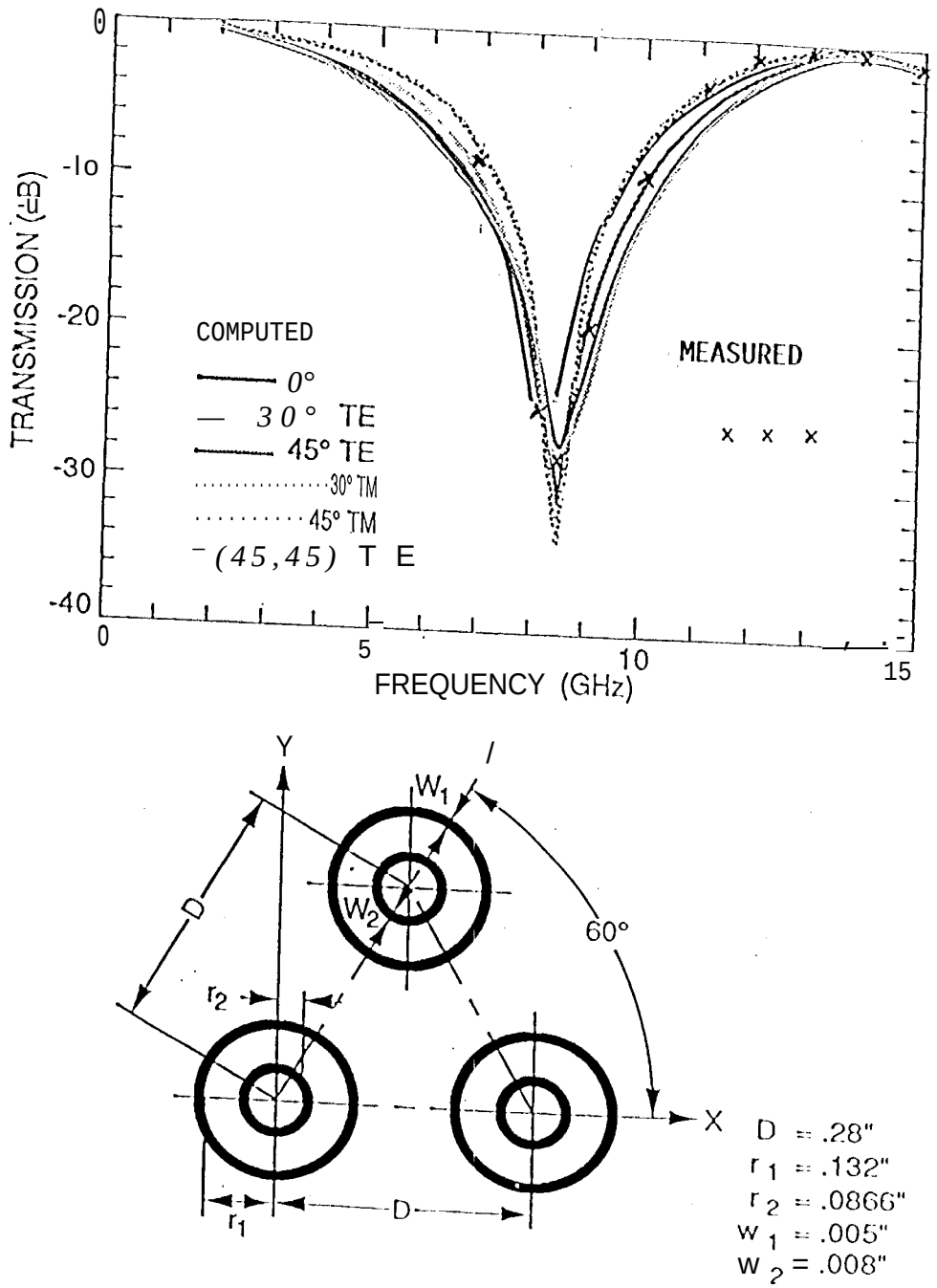

Figure 9. Design and transmission performance of the three-frequency FSS with double-ring element.

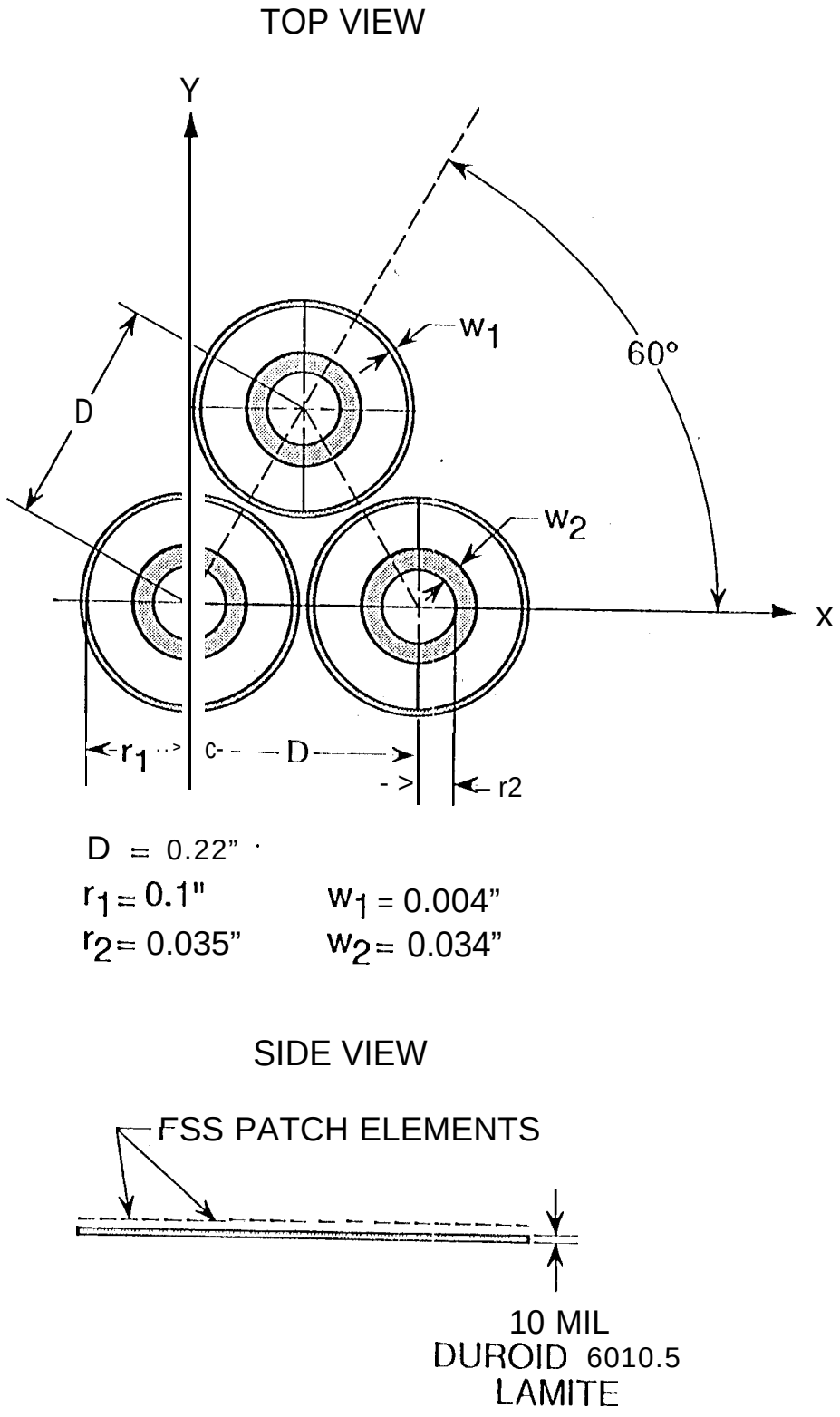

Figure 10. Configuration of a double-ring FSS on a 10 mil thick Duroid 6010.5 substrate.

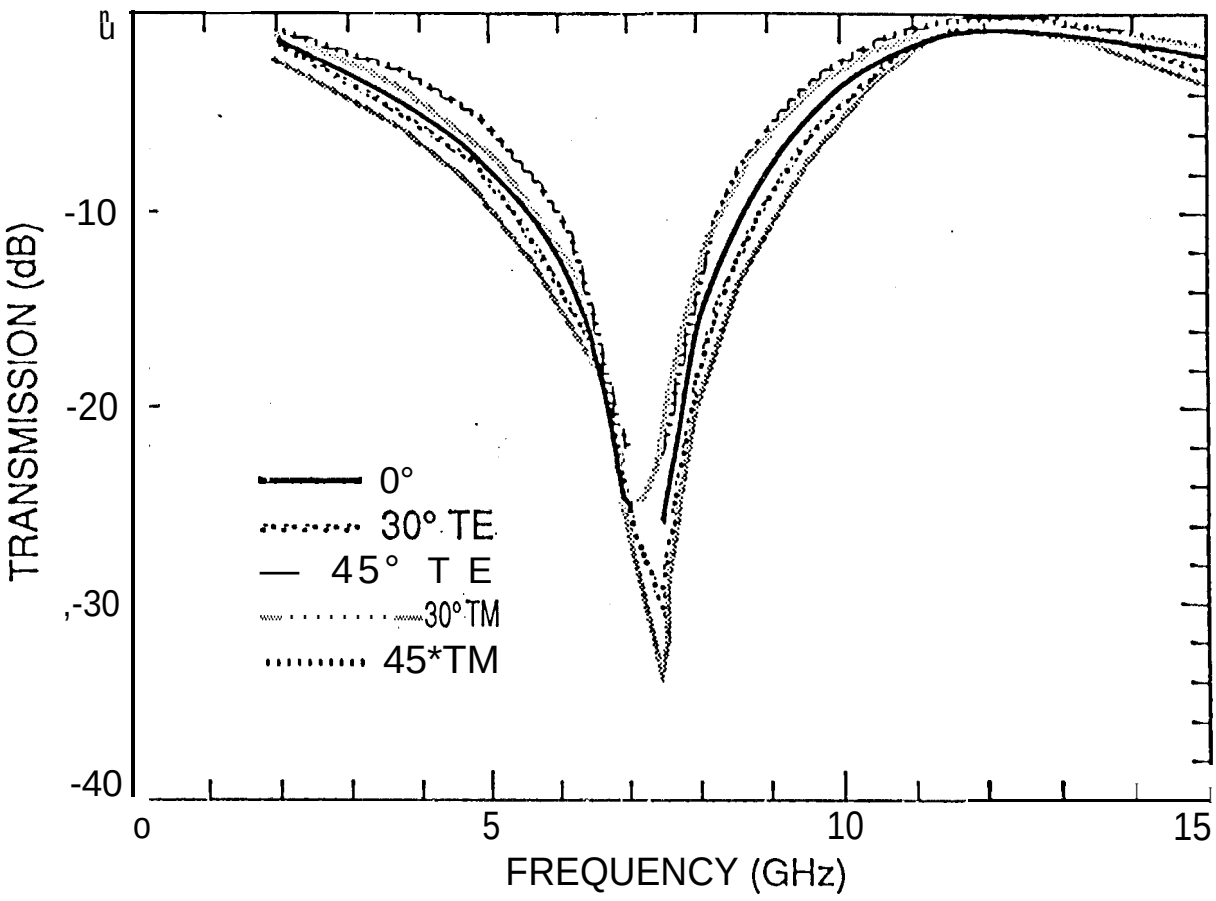

Figure 11. Computed transmission performance of the double ring element FSS of Figure 10.

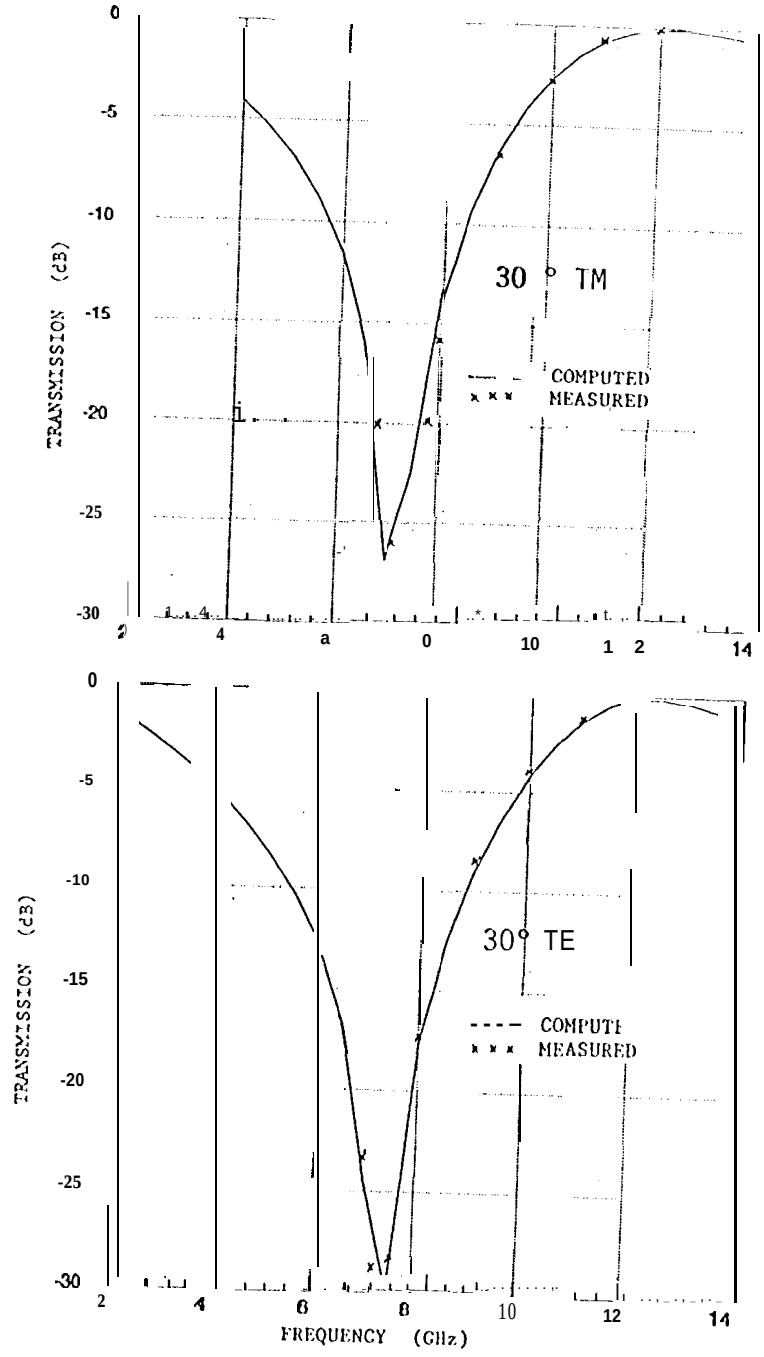

Figure 12 Comparison between measured and computed transmission performance Of the double ringelement FSS of Fig. 10.

FIGURE 13. TRANSMISSION PERFORMANCE OF THE SINGLE SCREEN FSS WITH DOUBLE RING ELEMENT OF FIGURE 10.

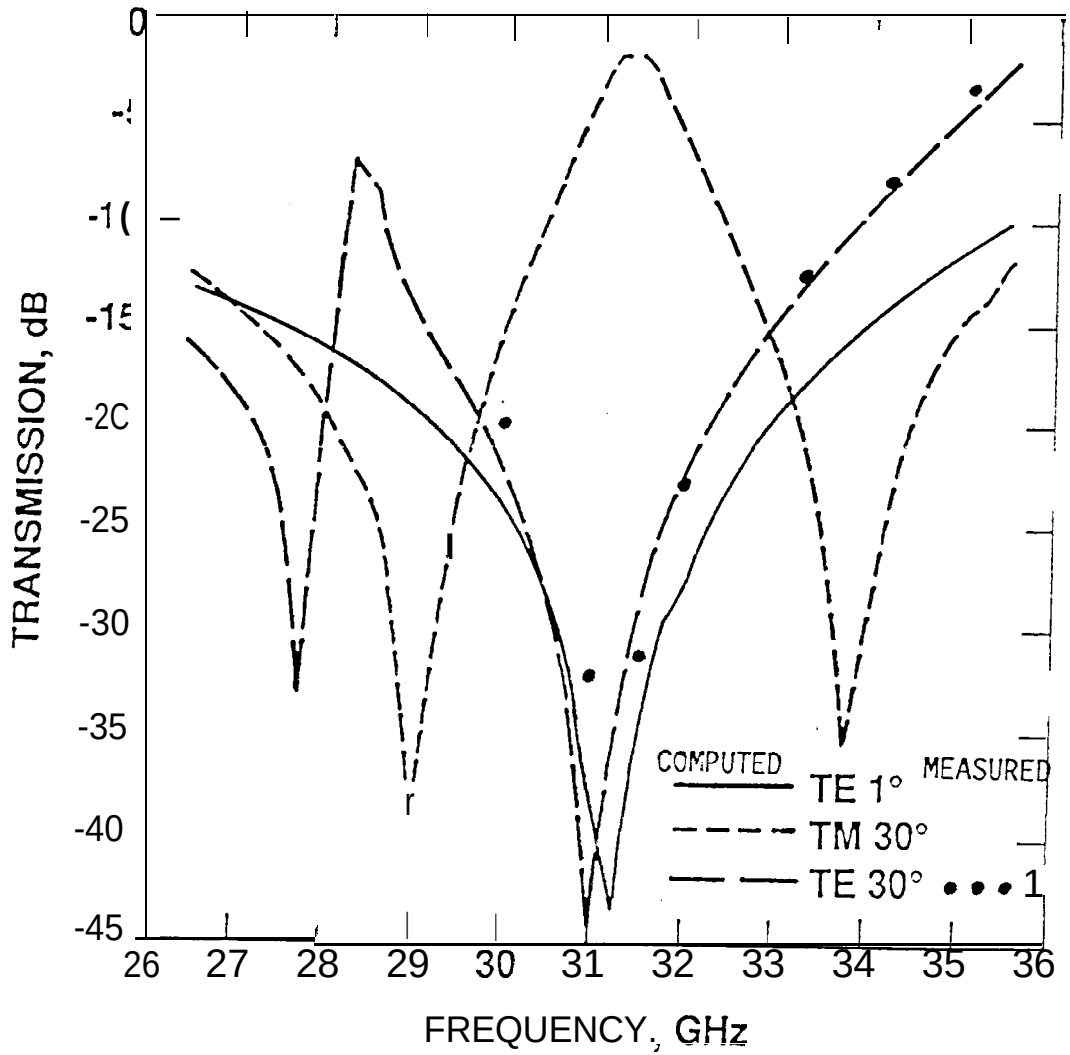

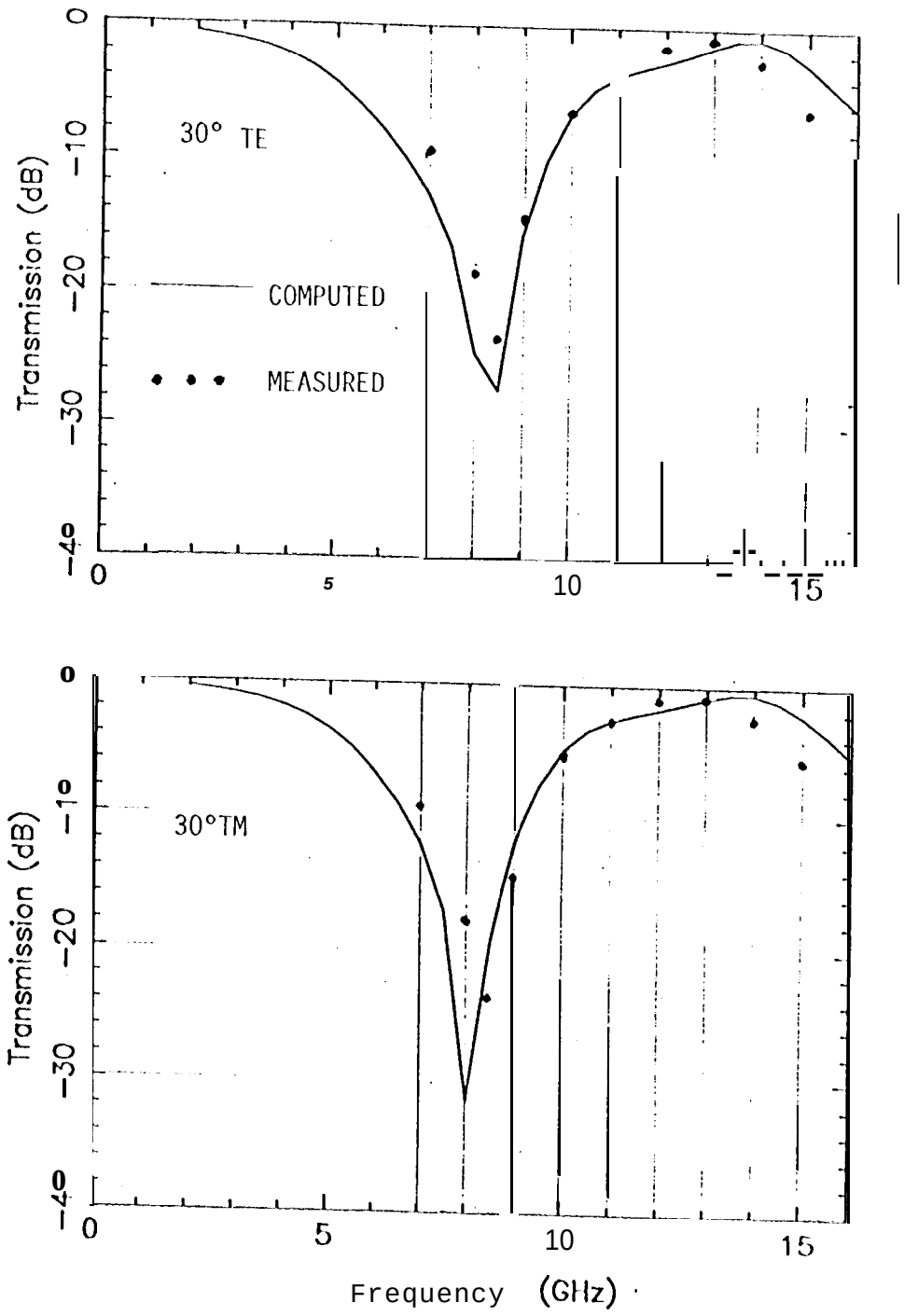

FIGURE 14. COMPARISON **OF COMPUTED AND MEASURED TRANSMISSION CHARACTERISTICS OF THE INTEGRATED DOUBLE SCREEN FSS WITH 0.75" THICK KEVLAR HONEYCOMB SANDWICH.**